Christelle Marminon, Christian Werner, Alexander Gast, Lars Herfindal, Johana Charles, Dirk Lindenblatt, Dagmar Aichele, Angélique Mularoni, Stein Ove Døskeland, Joachim Jose, Karsten Niefind and Marc Le Borgne*

Exploring the biological potential of the brominated indenoindole MC11 and its interaction with protein kinase CK2

https://doi.org/10.1515/hsz-2024-0160
Received December 15, 2024; accepted February 5, 2025; published online March 24, 2025

Abstract: Protein kinase CK2 is a promising therapeutic target, especially in oncology. Over the years, various inhibitors have been developed, with polyhalogenated scaffolds emerging as a particularly effective class. Halogens like bromine and chlorine enhance inhibitor stability by forming additional interactions within the ATP pocket. Among halogenated scaffolds, benzotriazole and benzimidazole have led to potent molecules such as 4,5,6,7-tetrabromo-1*H*-benzotriazole (IC_{50} = 300 nM) and 4,5,6,7-tetrabromo-2-(dimethylamino) benzimidazole (IC_{50} = 140 nM). Modifications, including 4,5,6-tribromo-7-ethyl-1*H*-benzotriazole (IC_{50} = 160 nM), further improved activity. Changing scaffolds while retaining halogens has enabled design of new inhibitors. Flavonols, dibenzofuranones, and the indeno[1,2-*b*]indole scaffold are key examples. Halogenation of the reference molecule 5-isopropyl-5,6,7,8-tetrahydroindeno[1,2-*b*]indole-9,10-dione (**4b**, IC_{50} = 360 nM) significantly boosted potency. The study focused on introducing four halogens, yielding to the compound 1,2,3,4-tetrabromo-5-isopropyl-5,6,7,8-tetrahydroindeno [1,2-*b*]indole-9,10-dione (**MC11**), with an IC_{50} of 16 nM. Co-crystallography revealed how bromine atoms enhance binding, and **MC11** demonstrated strong *in cellulo* activity, particularly against leukemic cell lines like IPC-Bcl2.

Keywords: halogenoindeno[1,2-*b*]indole; protein kinase CK2; CK2α; CK2α′; co-crystallisation; leukemia cells

Christelle Marminon and Christian Werner contributed equally to this work.

***Corresponding author: Marc Le Borgne**, Small Molecules for Biological Targets Team, Centre de Recherche en Cancérologie de Lyon, Centre Léon Bérard, CNRS 5286, INSERM 1052, Université Claude Bernard Lyon 1, Univ. Lyon, F-69373 Lyon, France, E-mail: marc.le-borgne@univ-lyon1.fr. https://orcid.org/0000-0003-1398-075X

Christelle Marminon, Johana Charles and Angélique Mularoni, Small Molecules for Biological Targets Team, Centre de Recherche en Cancérologie de Lyon, Centre Léon Bérard, CNRS 5286, INSERM 1052, Université Claude Bernard Lyon 1, University of Lyon, F-69373 Lyon, France, E-mail: christelle.marminon-davoust@univ-lyon1.fr (C. Marminon), johana.charles@univ-lyon1.fr (J. Charles), angelique.mularoni@univ-lyon1.fr (A. Mularoni). https://orcid.org/0000-0002-4043-3949 (C. Marminon). https://orcid.org/0009-0009-5390-6926 (J. Charles). https://orcid.org/0000-0002-3289-805X (A. Mularoni)

Christian Werner, Dirk Lindenblatt and Karsten Niefind, Department of Chemistry and Biochemistry, Institute of Biochemistry, University of Cologne, Zülpicher Str. 47, D-50674 Köln, Germany, E-mail: dirk.lindenblatt@freenet.de (D. Lindenblatt), Karsten.Niefind@uni-koeln.de (K. Niefind). https://orcid.org/0000-0001-5263-4994 (C. Werner). https://orcid.org/0000-0002-5561-1082 (D. Lindenblatt). https://orcid.org/0000-0002-0183-6315 (K. Niefind)

Alexander Gast, Dagmar Aichele and Joachim Jose, Institute of Pharmaceutical and Medicinal Chemistry, University of Münster, PharmaCampus, Corrensstraße 48, D-48149 Münster, Germany, E-mail: alexander.gast@uni-muenster.de (A. Gast), dagmar.aichele@uni-muenster.de (D. Aichele), joachim.jose@uni-muenster.de (J. Jose). https://orcid.org/0009-0001-1999-9155 (A. Gast). https://orcid.org/0000-0001-5937-0450 (D. Aichele). https://orcid.org/0000-0002-0666-2676 (J. Jose)

Lars Herfindal, Department of Clinical Science, University of Bergen, N-5009 Bergen, Norway, E-mail: Lars.Herfindal@uib.no. https://orcid.org/0000-0003-0353-3614

Stein Ove Døskeland, Department of Biomedicine, University of Bergen, N-5009 Bergen, Norway, E-mail: stein.ove.doskeland@gmail.com. https://orcid.org/0000-0002-4009-4756

1 Introduction

Protein kinase CK2 is a ubiquitously expressed serine/threonine protein kinase present in all eukaryotic cells. This tetrameric holoenzyme consists of two catalytic subunits (α and/or α′) and two regulatory subunits (β) and is constitutively active. CK2 can phosphorylate hundreds of protein substrates (Litchfield 2003) and is implicated in most biological processes, including in a wide range of human diseases (Borgo et al. 2021), such as neurodegenerative disorders (Castello et al. 2017), viral infections, namely SARS-CoV-2 (Quezada Meza and Ruzzene 2023), and cancer (Trembley et al. 2023). In the latter case, CK2 was reported to regulate various signaling pathways associated with cancer progression and response to damage signals (Chen et al. 2023; Meggio and Pinna 2003). CK2 is overexpressed in numerous tumor cells, which exhibit a dependency on CK2, referred to as a “non-oncogene addiction” (Ruzzene and

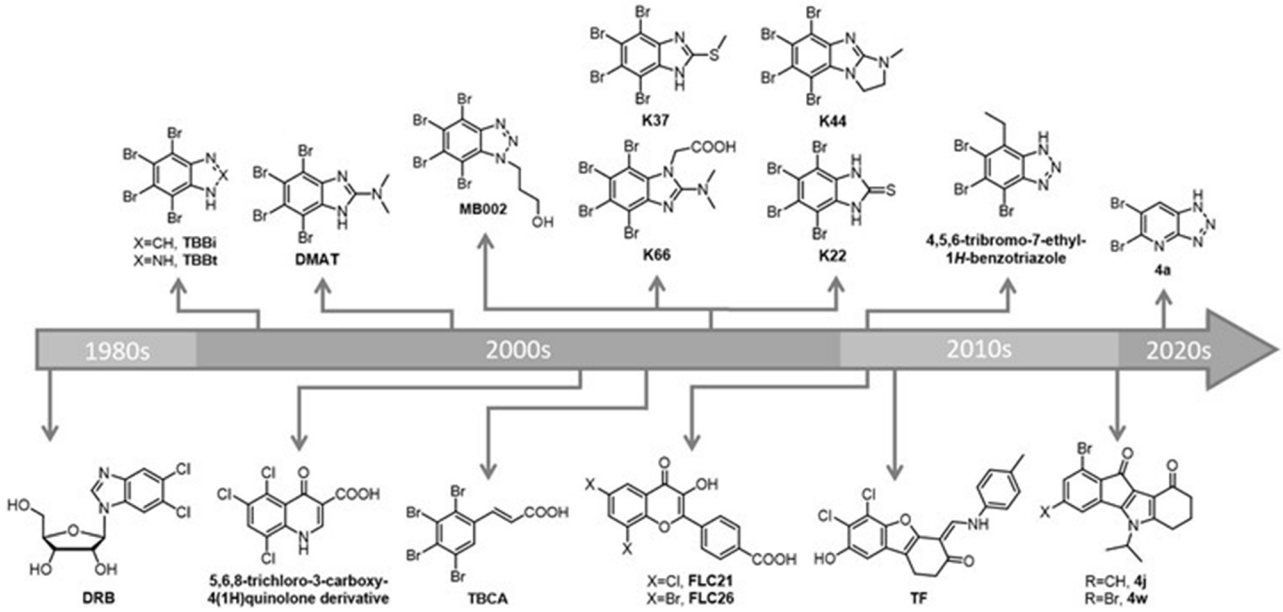

Figure 1: A timeline of potent halogenated inhibitors of protein kinase CK2.

Pinna 2010). This makes CK2 a promising target for antitumor therapies (Borgo et al. 2021; Chen et al. 2023), and numerous scaffolds have thus been employed in the development of CK2 inhibitors (Cozza 2017), notably scaffolds harboring halogen substituents (e.g., Br, Cl, I). Over the last four decades, the design of CK2 inhibitors has progressively advanced (Figure 1), resulting in particular in the incorporation of bromine and chlorine substituents on various (hetero)cyclic scaffolds.

The very first CK2 inhibitor featuring halogens was 5,6-dichloro-1-β-D-ribofuranosylbenzimidazole (**DRB**, IC_{50} = 15,000 nM) (Zandomeni et al. 1986). This discovery paved the way for the development of 4,5,6,7-tetrabromo-1*H*-benzotriazole (**TBBt**, IC_{50} = 300 nM) (Sarno et al. 2001; Zień et al. 2005), 4,5,6,7-tetrabromo-2-(dimethylamino)benzimidazole (**DMAT**, IC_{50} = 140 nM) (Pagano et al. 2004a,b), 4,5,6,7-tetrabromo-1*H*-benzimidazole (**TBBi**, IC_{50} = 1,300 nM) (Zień et al. 2005), and tetrabromocinnamic acid (**TBCA**, IC_{50} = 110 nM) (Pagano et al. 2007). Indeed, benzimidazole and benzotriazole scaffolds have been at the heart of numerous studies aimed at developing potent and selective inhibitors of protein kinase CK2. Compounds such as 1-carboxymethyl-2-dimethylamino-4,5,6,7-tetrabromobenzimidazole (**K66**, IC_{50} = 500 nM) (Pagano et al. 2008), 3-(4,5,6,7-tetrabromo-1*H*-benzotriazol-1-yl)propan-1-ol (**MB002**, IC_{50} = 320 nM) (Bretner et al. 2008) and 4,5,6-tribromo-7-ethyl-1*H*-benzotriazole (IC_{50} = 160 nM) (Makowska et al. 2011) illustrate the importance of polybrominated groups to interact with CK2, strengthening the binding through hydrophobic and halogen interactions. The year 2008 was also marked by other polybrominated derivatives based on *o*-phenylenediamine, for instance the compounds **K22** (K_i = 200 nM), **K37** (K_i = 70 nM) and **K44** (K_i = 100 nM) (Mazzorana et al. 2008; Winiewska-Szajewska et al. 2021). In addition, compounds related to benzotriazole and benzimidazole were developed by incorporating a nitrogen atom into the benzene ring, resulting in halogenated azolo[4,5-*b*]pyridine-type compounds. Compound **4a** proved to be the most active in inhibiting CK2 (IC_{50} = 2,560 nM) (Chojnacki et al. 2021).

The introduction of halogens such as bromine and chlorine in the design of CK2 inhibitors gradually continued, replacing the benzimidazole and benzotriazole motifs with other scaffolds such as quinolones (5,6,8-trichloro-4-oxo-1,4-dihydroquinoline-3-carboxylic acid, IC_{50} = 300 nM) (Golub et al. 2006), flavonols, exemplified by the compounds **FLC21** and **FLC26** (IC_{50} = 40 and 9 nM, respectively) (Golub et al. 2011), and dibenzofuranones, including the molecule **TF** (IC_{50} = 29 nM) (Gotz et al. 2012; Schnitzler et al. 2018) have brought to light new CK2 inhibitors. Finally, some halogenated CK2 inhibitors that contain the **indeno[1,2-*b*]indole** structural motif (Rongved et al. 2013), particularly two mono- and di-brominated inhibitors, **4j** and **4w** (IC_{50} = 140 and 110 nM, respectively) (Haidar et al. 2020), should be highlighted as they display a greater inhibitory activity than the reference molecule **4b** (IC_{50} = 360 nM) (Hundsdörfer et al. 2012).

Halogens, especially bromine atoms, play a key role in these systems due to their ability to form halogen bonds with specific residues within the active sites of CK2α and CK2α′. This has paved the way for fine-tuned chemistry aimed at improving the pharmacological properties of these

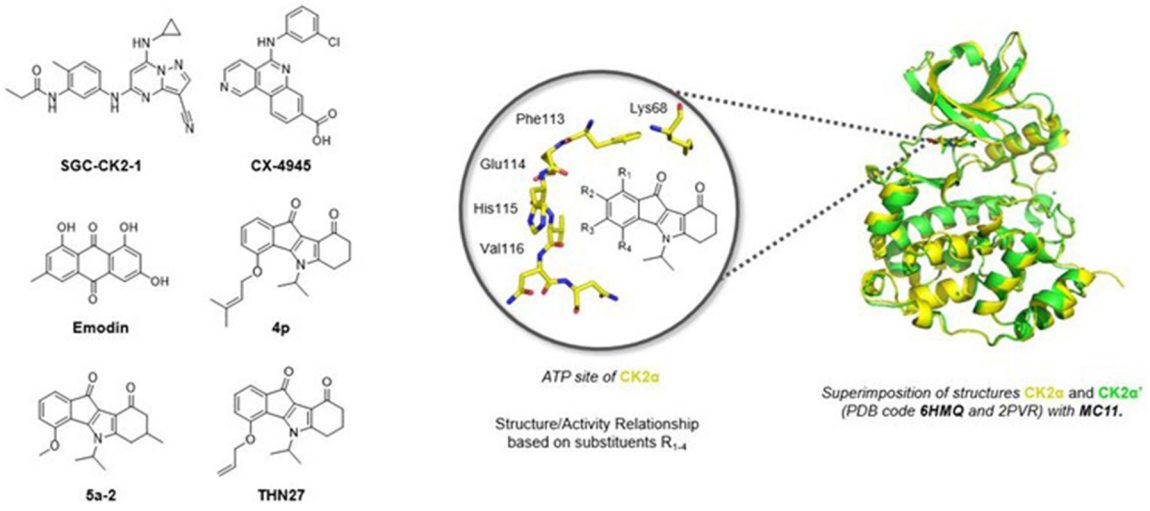

Figure 2: General structure of reference inhibitors and emerging tetrahalogenated indeno[1,2-*b*]indoles.

compounds. To enhance the efficacy of existing indeno[1,2-*b*]indoles as CK2 inhibitors, including **4j** and **4w** (Figure 1), and **4p**, **5a-2** and **THN27** (Figure 2), we present the synthesis and evaluation of two novel tetrahalogenated derivatives, **MC11** and **MC14**, inspired by the structural motifs of **TBBt**. All structures of reference compounds used in this article are also described in Figure 2.

2 Results and discussion

2.1 Chemical synthesis of halogenated indeno[1,2-*b*]indoles

Tetrabromo- and tetrachloroindeno[1,2-*b*]indole-9,10-diones **MC11** and **MC14** were quickly synthetized according to the previously reported two-step procedure (Figure 3) (Haidar et al. 2020; Hemmerling and Reiss 2009). First, the corresponding tetrahalogenoninhydrin **MC2** was coupled with the isopropylenaminone **MC3** (Hundsdörfer et al. 2012) in methanol (MeOH) to afford the dihydroxylated derivative **MC4**, which was then subjected to a dedihydroxylation step using tetraethylthionylamide (TETA).

Tetrahalogenoninhydrins **MC2** were prepared through the rapid microwave-assisted selenium oxidation of the corresponding tetrahalogenoindane-1,3-diones **MC1** (Marminon et al. 2015), in turn obtained from the corresponding phthalic anhydrides, according to the method described by Bouzina et al. (2021).

2.2 *In silico* physicochemical properties and cell viability of halogenoindeno[1,2-*b*] indole-9,10-diones

Lipinski's rule of five (Ro5), established in 1997 (Lipinski et al. 2001), provides a founding guideline for assessing the drug-likeness or pharmacokinetic suitability of chemical compounds. This rule is widely recognized in pharmaceutical research for evaluating whether a compound is likely to be orally active as a drug. The parameters include molecular weight (MW), less than 500 g/mol; hydrogen bond donors, no more than 5, typically involving hydroxyl (OH) or amine

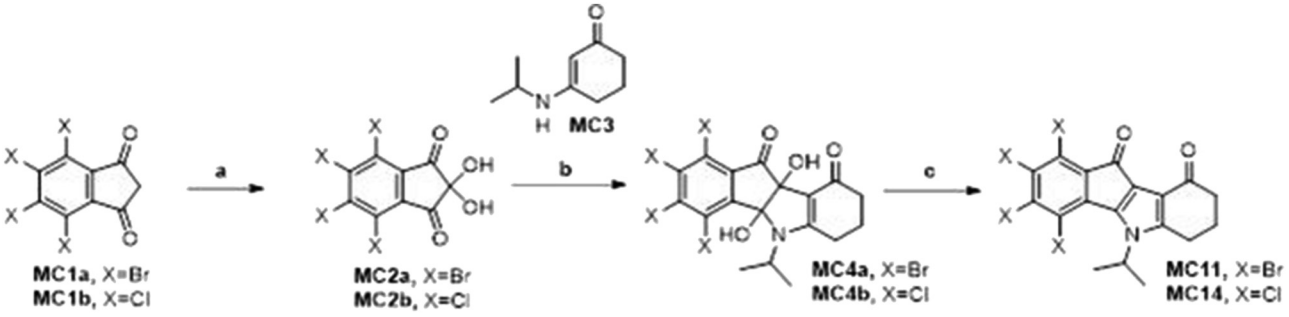

Figure 3: Synthesis of compounds used in this study. Reagents and conditions: (a) selenium dioxide, dioxane, water, microwave irradiation, 180 °C; (b) methanol, room temperature; (c) TETA, *N*,*N*-dimethylformamide, acetic acid, room temperature.

Table 1: *In silico* physicochemical properties and cell viability of halogenoindeno[1,2-*b*]indole-9,10-diones.

Cpd	Ro5				Water solubility Log S^b	TPSA (Å^2)
	MW (g/mol)	HBD	HBA	Log $P_{o/w}{}^a$		
4b	279.33	0	2	3.02	−3.58	39.07
4j	358.23	0	2	3.60	−4.49	39.07
4w	437.13	0	2	4.21	−5.40	39.07
MC11	594.92	0	2	5.34	−7.22	39.07
MC14	417.11	0	2	4.99	−5.96	39.07

[a]Consensus Log $P_{o/w}$, average of all five predictions; [b]ESOL: topological method implemented from Delaney (2004).

(NH) groups; hydrogen bond acceptors, no more than 10, usually oxygen (O) or nitrogen (N) atoms; LogP (lipophilicity), the partition coefficient should be below 5. We have supplemented the Rule of Five (Ro5) data with two additional parameters, namely water solubility and *topological polar surface area* (TPSA), whose value must be below 140 Å^2.

Results summarized in Table 1 provide insights into the compliance or not of our compounds with these parameters. We note that the compound **MC11** does not meet the MW parameter, with a value exceeding 500 g/mol. Moreover, its solubility is also limited (Log *S* = 7.22). This *in silico* solubility data was confirmed during the cytotoxicity evaluation assay. Due to its low solubility (not soluble in 20 mM DMSO), its intrinsic toxicity was evaluated on human lung fibroblast MRC5 cells at 4 mM. Its half-maximal inhibitory growth concentration (GI_{50}) was 20 µM.

2.3 Inhibition of CK2 *in vitro*

In order to investigate the effects of full halogenation at the A-ring of the indeno[1,2-*b*]indoles on their CK2 inhibitory activity, IC_{50} values were determined for the **MC11** and **MC14** compounds (Table 2). Both exhibited a remarkable inhibitory activity towards CK2$\alpha_2\beta_2$ with IC_{50} values of 16 nM and 29 nM, respectively. Compared to compounds with a lower degree of halogenation, such as those previously tested (Haidar et al. 2020; Hundsdörfer et al. 2012), it seems that full halogenation results in stronger inhibition. Given the higher

Table 2: Inhibitory effect of selected indeno[1,2-*b*]indoles and prominent CK2-inhibitors as determined in the capillary electrophoresis based CK2-activity assay.

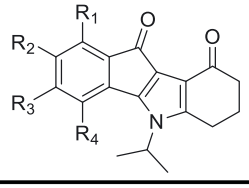

Compound	R_1	R_2	R_3	R_4	IC_{50} (nM)			Reference
					CK2α	CK2α′	CK2$\alpha_2\beta_2$	
4b	H	H	H	H			360.0	Hundsdörfer et al. (2012)
4j	Br	H	H	H			140.0	Haidar et al. (2020)
4w	Br	H	Br	H			110.0	Haidar et al. (2020)
MC11	Br	Br	Br	Br	24	19	016.0	–
MC14	Cl	Cl	Cl	Cl			029.0	–
TBBt	–	–	–	–			060.0	Jabor Gozzi et al. (2015)
4p	–	–	–	–			025.0	Jabor Gozzi et al. (2015)
5a-2	–	–	–	–			025.0	Birus et al. (2022)
THN27	–	–	–	–	607	273	130.0	Lindenblatt et al. (2019)
CX-4945	–	–	–	–			003.7	Jabor Gozzi et al. (2015)
SGC-CK2-1	–	–	–	–			029.0	–

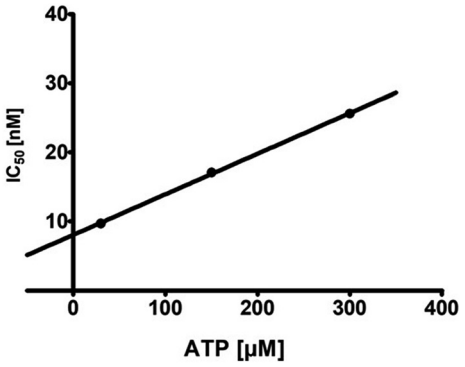

Figure 4: IC_{50} values for **MC11** plotted against the corresponding ATP concentration. A linear slope was obtained and its *Y*-axis intersection was taken as the K_i value. IC_{50} values were determined with the standard kinase activity assay by capillary electrophoresis in a sample size of $n = 3$.

potency of brominated **MC11** in comparison to the chlorinated **MC14**, and that it is the most potent indeno[1,2-*b*] indole-based CK2 inhibitor known to date, we decided to focus on **MC11** for further characterization. Although less potent than **CX-4945**, other prominent CK2 inhibitors, such as **SGC-CK2-1** and **TBBt**, tested here as reference compounds, exhibited slightly lower inhibitory effects compared to **MC11** (Table 2).

In order to determine the K_i value of **MC11** for the CK2 holoenzyme, IC_{50} values were measured with differing ATP concentrations. The following ATP concentrations, 30 µM, 150 µM and 300 µM led to IC_{50} values of 9.7 nM, 17 nM and 25.6 nM, respectively, resulting in a linear slope (Figure 4). This clearly indicated an ATP-competitive mode of action of **MC11**. The intersection of the linear slope with the *Y*-axis was taken as the K_i value, which turned out to be 8.1 nM.

We next wondered whether **MC11** has different affinities towards CK2α and CK2α′, and determined its IC_{50} value in each case. The similar levels obtained, namely 24 nM and 19 nM, respectively, suggested that **MC11** has no specificity for either subunit. Moreover, **MC11** inhibited both catalytic subunits to the same extent as the holoenzyme

Table 3: K_m and V_{max} of CK2α with ATP at different concentrations of **MC11**.

MC11 concentration [nM]	K_m [µM]	V_{max} [nmol/min]
0	7.4 ± 2.8	1.01 ± 0.25
020	14.2 ± 4.7	1.06 ± 0.10
100	63.8 ± 23.4	1.13 ± 0.18

$CK2\alpha_2\beta_2$. To verify the mode of inhibition of **MC11** on CK2α, its activities were evaluated at different concentrations of **MC11** and ATP, and plotted according to Hanes-Woolf (Figure 5A). Then, the Hanes-Woolf Plot was used to determine K_m and V_{max} of ATP with CK2α at differing **MC11** concentrations. As shown in Table 3, K_m increased with increasing ATP concentrations, whereas V_{max} remained the same. Hence, this confirmed the ATP-competitive mode of action of **MC11**. K_m and V_{max} values obtained from the primary Hanes-Woolf plot were applied to a secondary plot as shown in Figure 5B. Here, the intersection of the linear slope and the *X*-axis generated the $-K_i$ value according to the Hanes-Woolf plot, giving rise to a K_i of 9.5 nM for **MC11** with CK2α, almost identical to that determined for the $CK2\alpha_2\beta_2$ holoenzyme.

2.4 Crystal structures of MC11 in complex with CK2α and CK2α′

In order to get insights into the binding of **MC11** to the isoenzymes of CK2 catalytic subunit, we determined two crystal structures of **MC11** in complex with CK2α and one in complex with CK2α′ and refined them to acceptable R values (Table S1). The better resolved CK2α/**MC11** structure had a resolution of 1.7 Å, while the CK2α′/**MC11** even reached atomic resolution (1.04 Å). We use these two structures (columns 2 and 4 of Table S1) for the subsequent discussion. In the second (less well resolved) CK2α/**MC11** structure, obtained under low-salt crystallization conditions, no

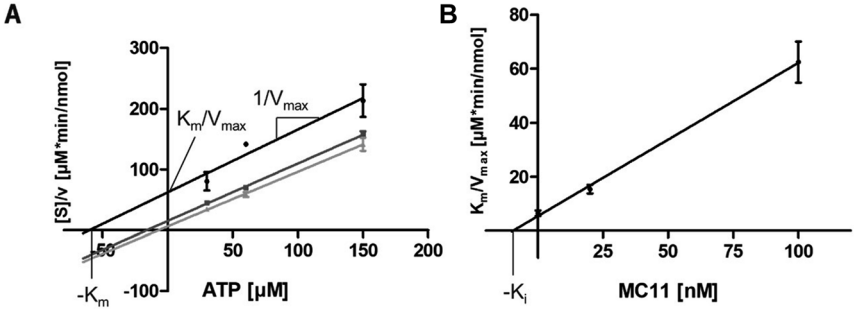

Figure 5: CK2α activities obtained at different concentrations of **MC11** and ATP plotted according to Hanes-Woolf. Panel (A) shows the primary Hanes-Woolf plot, which was used to determine K_m and V_{max} with different **MC11** concentrations (● 100 nM **MC11**, ■ 20 nM **MC11**, ▲ 0 nM **MC11** (DMSO)). The *Y*-axis intercept was used to determine K_m/V_{max}, which was applied in the secondary Hanes-Woolf plot shown in panel (B). The secondary plot was used to determine the K_i value of **MC11** for CK2α.

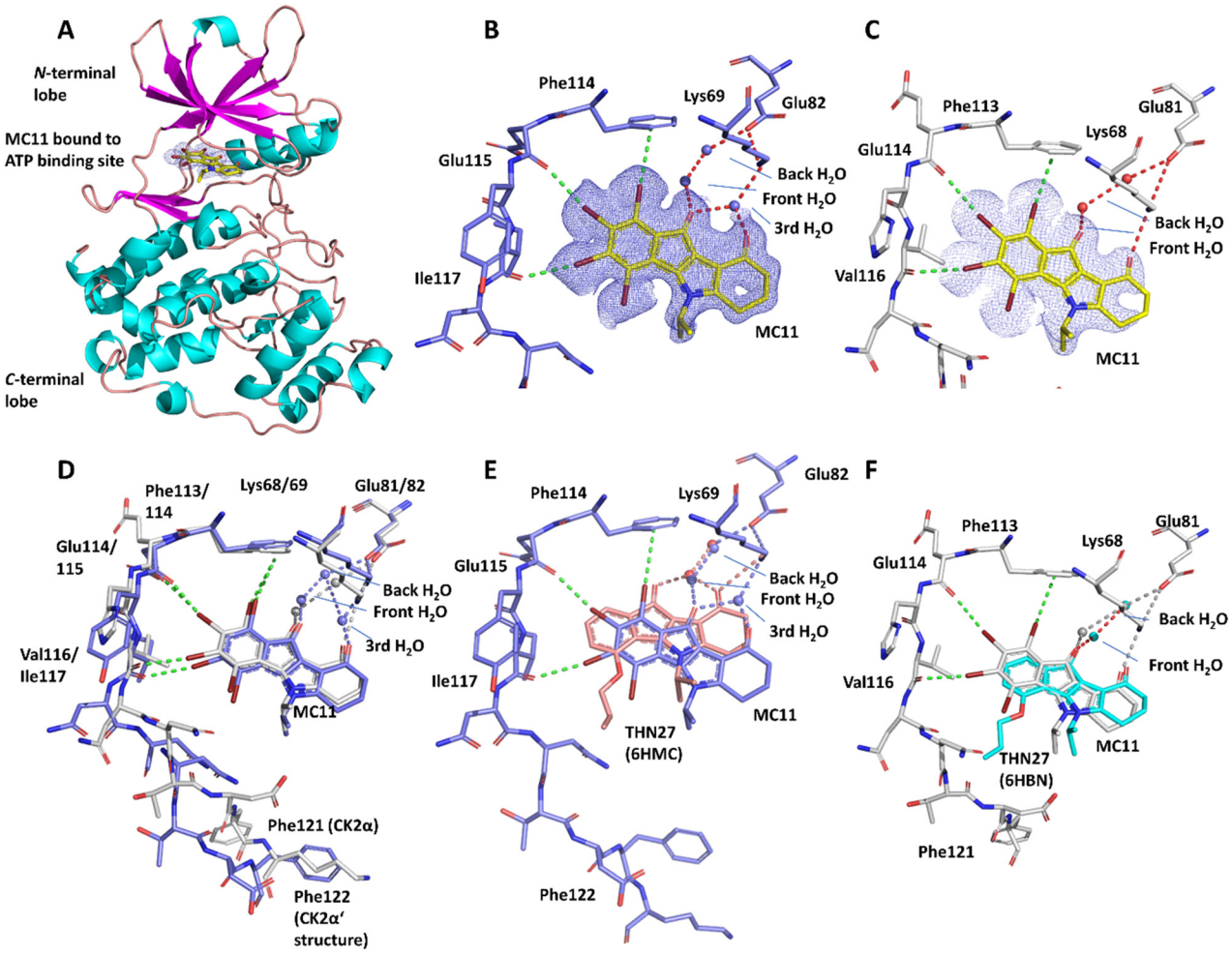

Figure 6: Structures of **MC11** in complex with CK2α and CK2α′. (A) Overview of the CK2α′/**MC11** complex structure. (B/C) **MC11** at the ATP site of CK2α′ (B) and CK2α (C); green dotted lines indicate halogen bonds and red dotted lines hydrogen bonds. (D) Local structural overlay of the CK2α/**MC11** (grey C-atoms) and the CK2α′/**MC11** (slate-blue C-atoms) complex structures. (E) Superimposition of the CK2α′/**MC11** structure and the CK2α′/**THN27** structure (PDB_ID 6HMC). (F) Superimposition of the CK2α/**MC11** structure and the CK2α/**THN27** structure (PDB_ID 6HBN). The pieces of electron density visible in parts A-C of the Figure were drawn with a cut-off level of 1.0 σ.

significant differences compared to the first one are visible; therefore, this structure is just documented in column 3 of Table S1 as well as in Figure S1, which illustrates the same features as discussed below. A structural overview illustrates that **MC11** binds to the canonical ATP/GTP binding site (Figure 6A).

The two bromo substituents at positions 2 and 3 of ring A form halogen bonds with the carbonyl oxygen atoms of Glu114 and Val116 in CK2α, and with Glu115 and Ile117 in CK2α′, respectively (Figure 6B and C), while the bromo substituent at position 1 of ring A is part of a π-halogen bond with the gatekeeper residue Phe113 (Phe114 in CK2α′). Only the fourth bromo substituent (at position 4 of ring A) is not involved in any halogen bond, but points towards the solvent. The ketonic oxo groups of the rings B and D establish water-mediated hydrogen bonds with the highly conserved residues Lys68 (Lys69 in CK2α′) and Glu81 (Glu82 in CK2α′). The water molecule facing the inhibitor was previously named “front water” and the water closer to the conserved glutamate was called “back water” (Hochscherf et al. 2017; Lindenblatt et al. 2019). In the CK2α′/**MC11** complex, a third water molecule is present contributing to the binding of **MC11** via hydrogen bond formation with the ketonic oxo group of ring D and with Lys69 (Figure 6B). An equivalent water molecule is absent in the CK2α/**MC11** complex (Figure 6C), where the ketonic oxo group of ring D is directly (without mediation by a water molecule) hydrogen-bonded to Lys68 (Figure 6D).

Which impact do the bromo substituents – via the halogen bonds they form – have on the binding mode of indenoindole-like CK2 inhibitors, as known so far from **4p**

(Hochscherf et al. 2017) as well as **THN27** and **AR18** (Lindenblatt et al. 2019)? All three are free of halogens and their orientations in the ATP site are dominated by hydrogen bonds. To answer the question formulated above, we overlaid the CK2α′/**MC11** structure and the CK2α/**MC11** structure with the equivalent complex structures with **THN27** (PDB_ID 6HMC: CK2α′/THN27; PDB_ID 6HBN: CK2α/**THN27**) (Figure 6E and F). The difference in the binding mode is particularly striking in CK2α′: Here, Figure 6E shows that the bromine atoms of **MC11** have shifted the indenoindole scaffold so strongly outwards and rotated it at the same time that ring D no longer makes direct polar contact with the enzyme and that space has been created for the aforementioned third water molecule. In the case of CK2α, the same shift and rotation of the indenoindole scaffold can be seen (Figure 6F); however, they are less pronounced, so that the space created is not sufficient for a third water molecule. Whether this subtle difference between CK2α and CK2α′ in the binding of **MC11** is due to their sequence difference in the hinge region (Figure 6D) and whether it can be expanded and utilized in the longer term to generate isoenzyme-selective inhibitors remains to be seen.

2.5 Cytotoxicity test on leukemia cell lines

The compounds were also tested on a panel of myeloid cancer cells, as well as on a chronic myeloid leukemia (CML) cell line and a non-cancerous cell line (Figures 7 and S2, Table S2). The CK2 inhibitor emodin was used as a reference compound for the bioactivity tests. The ability to induce apoptotic cell death was determined at 30 µM and 100 µM. The most active compounds were **4p** and **MC11**, which resulted in 100 % cell death in most acute myeloid leukemia (AML) cell lines. Interestingly, **MC11** was able to induce cell death in the cell line with enforced expression of Bcl-2 (IPC-Bcl2), whereas **4p** was less efficient towards these cells. The compounds **5a-2** and **TBBt** led to distinct responses toward the different AML/acute promyelocytic leukemia (APL) cell lines. For instance, **TBBt** did not induce apoptosis in MOLM-13 cells, but was efficient towards the MV4-11 and IPC-81 cell lines, even those with attenuated expression of p53 (MV4-11 shp53) or enforced expression of Bcl-2 (IPC-Bcl2). **MC14** was the least efficient compound, leading to less than 10 % apoptosis at 100 µM. In general, none of the compounds showed considerable activity towards the CML or normal rat kidney (NRK) cells, highlighting the potential of these compounds in AML therapy.

3 Conclusions

It seems clear that bromine enhances interactions between the indeno[1,2-*b*]indole A-ring and three amino acids of the ATP site (Phe113, Glu114 and Val116 in CK2α; Phe114, Glu115 and Ile117 in CK2α′), interactions that do not exist with **THN27**, for example (Figure 6F).

Then, these studies have not only enhanced our understanding of the structural interactions between inhibitors and CK2 but also provide new perspectives for optimizing our recent indeno[1,2-*b*]indole-based inhibitors (Birus et al. 2022) targeting protein kinase CK2. As part of the "XPLOR_CK2" partnership (https://anr.fr/en/funded-projects-and-impact/funded-projects/), we are working on

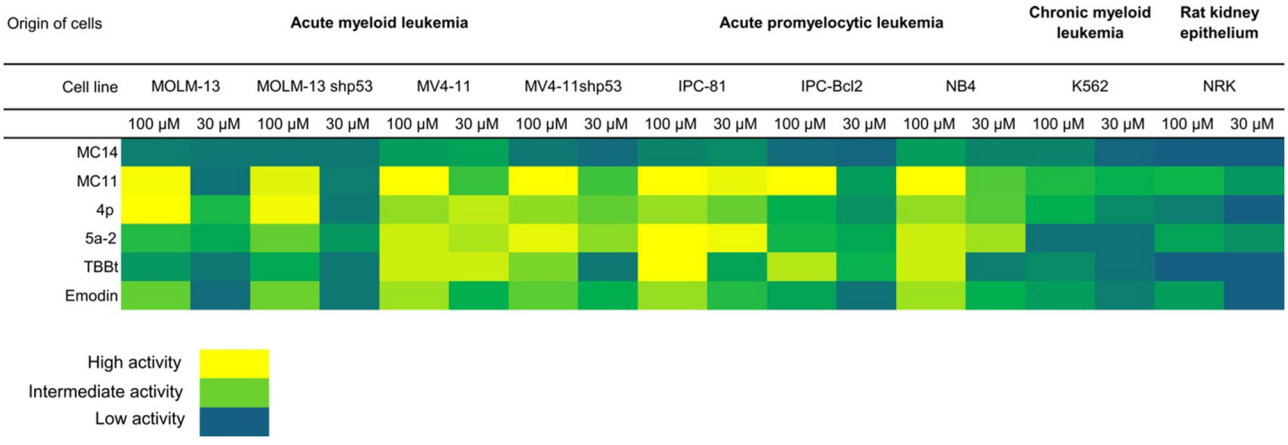

Figure 7: Cytotoxic potential of the CK2 inhibitors **MC11** and **MC14**. The CK2 inhibitor emodin was included as a reference compound. The cells were incubated with the given concentrations of the compounds for 24 h, then fixed and the DNA stained with the DNA-specific dye Hoechst 33342, and the percent of apoptotic cells was determined by microscopic evaluation of surface and nuclear morphology. See the materials and methods Section 4.7 for experimental details.

the development of a new generation of bivalent inhibitors (commonly referred to as type V inhibitors). Building on the success of TBBt as a warhead for the ATP-binding pocket (Lindenblatt et al. 2022), we now have additional options (e.g., **MC11**) to guide our drug design. **MC11** is also being further investigated for its potential to inhibit the human ATP-binding cassette *transporter ABCG2.*

4 Materials and methods

4.1 Chemistry

4.1.1 General

Chemicals are named according to IUPAC nomenclature. All of the reagents were purchased from Sigma-Aldrich and Thermo-Fisher Scientific.

4,5,6,7-Tetrachloroindane-1,3-dione **MC1b** was prepared according to the literature (Allen et al. 2008). Syntheses of 4,5,6,7-tetrabromo-2,2-dihydroxyindane-1,3-dione (**MC2a**) and enaminone **MC3** were already described (Bouzina et al. 2021 for **MC2a**, Jabor Gozzi et al. 2015 for **MC3**).

Microwave reactions were conducted using a Biotage Initiator Microwave synthesizer 2.0440 W. Melting points were determined on an Electrothermal 9200 capillary apparatus. The IR spectra were recorded on a PerkinElmer Spectrum Two IR spectrometer. The ^{1}H and ^{13}C NMR spectra were recorded at 400 MHz on a Bruker DRX 400 spectrometer or a Jeol ECZ 400 spectrometer. Chemical shifts are expressed in ppm (δ) downfield from internal tetramethylsilane and coupling constants J are reported in hertz (Hz). The following abbreviations are used: s, singlet; bs, broad singlet; d, doublet; t, triplet; dt, doubled triplet; q, quartet; qui, quintuplet; sept, septuplet; m, multiplet; Cquat, quaternary carbons. The mass spectra were performed by direct ionization (EI or CI) on a ThermoFinnigan MAT 95 XL apparatus.

Chromatographic separations were performed on silica gel columns by column chromatography (Kieselgel 300e400 mesh). All reactions were monitored by TLC on GF254 plates that were visualized under a UV lamp (254 nm). Solvent evaporation was performed under vacuum with a rotating evaporator. The purity of the final compounds (greater than 95 %) was determined by uHPLC/MS on an Agilent 1290 system using an Agilent 1290 Infinity ZORBAX Eclipse Plus C18 column (2.1 mm × 50 mm, 1.8 mm particle size) or a Poroshell 120 Agilent infinity lab (2.1 mm × 50 mm, 2.7 mm particle size) with a gradient mobile phase of H_2O/CH_3CN (90:10, *v*/*v*) with 0.1 % formic acid to H_2O/CH_3CN (10:90, *v*/*v*) with 0.1 % formic acid at a flow rate of 0.5 ml/min, with UV monitoring at the wavelength of 254 nm with a run time of 10 min.

4.1.2 Synthesis of tetrahalogenoindeno[1,2-*b*]indole-9,10-diones MC11 and MC14

4.1.2.1 4,5,6,7-Tetrachloro-2,2-dihydroxyindane-1,3-dione (MC2b)

A sealed-pressurized reaction vessel (5 ml) equipped with a magnetic stirrer and charged with 4,5,6,7-tetrachloroindane-1,3-dione **MC1b** (285 mg, 1.00 mmol), selenium dioxide (167 mg, 1.50 mmol), dioxane (3.8 ml) and two drops of water, was irradiated 5 min at 180 °C with a maximum of 400 W. The vessel was rapidly forced-air cooled to room temperature. The mixture was transferred to a round bottom flask, and the vessel washed with acetone. Silica was added to prepare a solid deposit. The volatile solvents were then evaporated *in vacuo* before purification by flash chromatography (ethyl acetate:cyclohexane, 1:2) to give the corresponding ninhydrin **MC2b** clearly recognizable as a brown solid (194 mg, 0.61 mmol, 61 %).

Mp > 148 °C, degradation. R_f (ethyl acetate:cyclohexane, 1:2): 0.21. IR υ (cm^{-1}): 3,370 (OH), 1,744 (C=O), 734 (C–Cl). ^{1}H NMR (400 MHz, DMSO-d_6): δ 7.84 (bs, 2H, OH). ^{13}C NMR (101 MHz, DMSO-d_6): 192.16 (2 C=O), 140.89 (Cquat), 134.10 (Cquat), 129.45 (Cquat), 87.22 ($C(OH)_2$). MS-ESI calcd for $C_9H_3Cl_4O_4$ $[M+Na]^+$ 314.8780, found: 314.8779.

4.1.2.2 1,2,3,4-Tetrabromo-4b,9b-dihydroxy-5-isopropyl-4b,5,6,7,8,9b-hexahydroindeno[1,2-*b*]indole-9,10-dione (MC4a)

A solution of tetrabromoninhydrin **MC2a** (634 mg, 1.28 mmol) and enaminone **MC3** (206 mg, 1.34 mmol) in methanol (25 ml) was stirred at room temperature for 24 h. The precipitate was then filtered and washed with diethyl ether (Et_2O) to obtain the corresponding dihydroxy derivative **MC4a**, clearly recognizable as an orange solid (594 mg, 0.95 mmol, 74 %).

Mp > 158 °C, degradation. R_f (ethyl acetate) 0.54. IR ν (cm^{-1}): 3,347 (OH), 1,717 (C=O), 1,758 (C=O), 1,163 (C–Br). ^{1}H NMR (400 MHz, DMSO-d_6): δ 7.00 (s, 1H, OH), 6.11 (s, 1H, OH), 4.76 (sept, J = 7.0 Hz, 1H, $C\underline{H}(CH_3)_2$), 2.76 (dt, 1H, J = 17.6, 5.5 Hz, 1H of CH_2), 2.43–2.35 (m, 1H, 1H of CH_2), 2.08–2.00 (m, 2H, CH_2), 1.85–1.69 (m, 2H, CH_2), 1.46 (d, J = 7.1 Hz, 3H, CH_3), 1.25 (d, J = 6.6 Hz, 3H, CH_3). ^{13}C NMR (101 MHz, DMSO-d_6): δ 193.48 (C=O), 189.92 (C=O), 167.65 (Cquat), 148.04 (Cquat), 137.00 (Cquat), 135.12, (Cquat), 132.58 (Cquat), 122.23 (Cquat), 120.58 (Cquat), 109.06 (Cquat), 96.12 (C–OH), 84.46 (C–OH), 46.64 (CH), 36.76 (CH_2), 25.05 (CH_2), 22.93 (CH_3), 22.41 (CH_3), 21.59 (CH_2). MS-ESI calcd for $C_{18}H_{16}Br_4NO_4$ $[M + H]^+$ 625.7802, found 625.7807.

4.1.2.3 1,2,3,4-Tetrachloro-4b,9b-dihydroxy-5-isopropyl-4b,5,6,7,8,9b-hexahydroindeno[1,2-*b*]indole-9,10-dione (MC4b)

A mixture of tetrachloroninhydrin **MC2b** (2.01 g, 6.37 mmol) and enaminone **MC3** (1.02 g, 6.68 mmol) in methanol (77 ml) was stirred at room temperature for 24 h. The precipitate was then filtered and washed with Et_2O to obtain the corresponding dihydroxy derivative **MC4b**, corresponding to a pale orange solid (1.15 g, 2.55 mmol, 40 %).

Mp 193 °C. R_f (dichloromethane:acetone, 9:1) 0.40. IR ν (cm^{-1}): 3419, 1740, 1,531, 723. ^{1}H NMR ($CDCl_3$, 400 MHz) δ: 7.12 (s, 1H, OH-4), 6.15 (bs, 1H, OH-9), 4.70 (sept, 1H, J = 7.0 Hz, C<u>H</u>$(CH_3)_2$), 2.78 (dt, 1H, J = 17.5, 5.4 Hz, 1H of CH_2), 2.49–2.41 (m, 1H, 1H of CH_2), 2.15–2.04 (m, 2H, CH_2), 1.93–1.74 (m, 2H, CH_2), 1.43 (d, 3H, J = 7.2 Hz, CH_3), 1.30 (d, 3H, J = 6.9 Hz, CH_3). ^{13}C NMR + DEPT (DMSO-d_6, 100 MHz) δ: 192.52 (C=O), 189.55, (C=O), 167.11 (Cquat), 150.27 (Cquat), 145.10 (Cquat), 138.41 (Cquat), 134.49 (Cquat), 132.03 (Cquat), 129.03, 128.07 (Cquat), 107.73 (Cquat), 95.90 (Cquat), 84.59 (Cquat), 45.90 (CH), 36.40 (CH_2), 24.88 (CH_2), 22.57 (CH_3), 22.38 (CH_3), 21.56 (CH_2). HRMS calcd for $C_{18}H_{16}Cl_4NO_4$ $[M + H]^+$ 449.9828, found 449.9817.

4.1.2.4 1,2,3,4-Tetrabromo-5-isopropyl-5,6,7,8-tetrahydroindeno[1,2-*b*]indole-9,10-dione (MC11)

A mixture of dihydroxy derivative **MC4a** (140 mg, 0.22 mmol), TETA (200 mg, 1.04 mmol), and acetic acid (0.04 ml) was dissolved in *N*,*N*-dimethylformamide (DMF) (0.2 ml) and stirred at room temperature for 24 h. Crushed ice was added and the mixture was stirred for 1 h. The precipitate was filtered, washed with water, Et_2O, and purified by column chromatography (dichloromethane:acetone, 9:1) to give a red solid (100 mg, 0.17 mmol, 76 %).

Mp 280 °C. R_f (dichloromethane:acetone, 9:1) 0.62. IR υ (KBr, cm^{-1}): 2,933, 1,714 (C=O), 1,655 (C=O), 552 (C–Br). ^{1}H NMR (400 MHz, $CDCl_3$ + drop DMSO-d_6): δ 5.52 (sept, 1H, J = 7.0 Hz, C<u>H</u>$(CH_3)_2$), 2.83 (t, 2H, J = 6.0 Hz, CH_2), 2.30 (m, 2H, J = 6.4 Hz, CH_2), 2.05–1.86 (m, 2H, CH_2), 1.44 (d, 6H, J = 6.9 Hz, $2CH_3$). ^{13}C NMR (100 MHz, $CDCl_3$ + drop DMSO-d_6): δ 191.48 (C=O), 177.90 (C=O), 152.32 (Cquat), 148.98 (Cquat), 139.59 (Cquat), 136.76 (Cquat), 134.71 (Cquat), 130.74 (Cquat), 123.32 (Cquat), 121.05 (Cquat), 119.41 (Cquat), 114.08 (Cquat), 52.12 (CH), 37.90 (CH_2), 25.55 (CH_2), 23.51 (CH_2), 21.98 (2 CH_3). HRMS calcd for $C_{18}H_{14}Br_4NO_2$: $[M+H]^+$ 591.7753 found: 591.7760.

4.1.2.5 1,2,3,4-Tetrachloro-5-isopropyl-5,6,7,8-tetrahydroindeno[1,2-*b*]indole-9,10-dione (MC14)

A mixture of dihydroxy derivative **MC4b** (1.14 g, 2.53 mmol), TETA (2.20 g, 11.5 mmol), and acetic acid (4.4 ml) was dissolved in DMF (16.3 ml) and stirred at room temperature for 24 h. Crushed ice was added and the mixture was stirred for 1 h. The precipitate was filtered, washed with water, Et_2O, and purified by column chromatography (dichloromethane:acetone, 9:1) to give a red solid (456 mg, 1.93 mmol, 43 %).

Mp 294 °C. R_f (dichloromethane:acetone, 9:1) 0.81. IR ν (cm^{-1}): 2,947 (CH), 1,718 (C=O), 1,666 (C=O), 726 (C–Cl). ^{1}H NMR ($CDCl_3$ + drop of DMSO-d_6, 400 MHz) δ: 5.50 (sept, 1H, J = 6.7 Hz, C<u>H</u>$(CH_3)_2$), 2.84 (t, 1H, J = 6.0 Hz, 2H, CH_2-6), 2.30 (t, 2H, J = 5.7 Hz, CH_2-8), 2.00–1.91 (m, 2H, CH_2-7), 1.49 (d, 3H J = 7.1 Hz, CH_3), 1.47 (d, 3H J = 7.1 Hz, CH_3). ^{13}C NMR + DEPT ($CDCl_3$ + drop of DMSO-d_6, 100 MHz) δ: 191.59 (C=O), 177.90 (C=O), 152.05 (Cquat), 148.20 (Cquat), 137.58 (Cquat), 135.69 (Cquat), 133.64 (Cquat), 133.30 (Cquat), 129.65 (Cquat), 123.27 (Cquat), 121.62 (Cquat), 119.24 (Cquat), 52.71 (CH), 38.01 (CH_2), 25.76 (CH_2), 23.72 (CH_2), 22.17 (2 CH_3). HRMS calcd for calcd for $C_{18}H_{13}Cl_4NNaO_2$: $[M+Na]^+$ 437.9593, found: 437.9597.

4.2 Determination of *in silico* physicochemical properties

In our study, we used the SwissADME web tool (http://www.SwissADME.ch/) to analyze various pharmacokinetic attributes, including molecular weight, LogP, hydrogen bonding capacity, rotatable bonds, and adherence to Lipinski's guidelines (Daina et al. 2017).

4.3 MRC5 cell viability assay

Cell viability assay was evaluated through the MTT colorimetric assay (Mosmann 1983). The assay was optimized for the cell lines used in the experiment. MRC5 cells (Lung Fibroblast Human CCL-171 ATCC) were plated in triplicate at a density of 6,000 cells/well in 96-well culture plates. Cells were incubated overnight at 37 °C in 5 % CO_2 in MEM (modified Eagle's medium) medium supplemented with 10 % FBS (fetal bovine serum). The following day, cells were treated with the compounds (1–40 μM) or with vehicle control (DMSO). After 72 h, the cells were incubated with 1 mg/ml of MTT (3-(4,5-dimethylthiazol-2-yl)-2,5-diphenyltetrazolium bromide, Sigma Aldrich) for 3 h at 37 °C. The medium was removed and 100 μl of 0.01 M HCl in isopropanol was added in each well for 15 min. Absorbance was measured by a plate reader at 570 nm and the value measured at 690 nm was subtracted. Data are presented as the mean ±SD of at least three independent experiments. GI_{50} value was calculated using GraphPadPrism.

4.4 Protein expression and purification

Purification of the $CK2\alpha_2\beta_2$ holoenzyme as applied in the *in vitro* kinase assay was performed as previously described (Gratz et al. 2010). For the purification of the catalytic subunits CK2α and CK2α′ a recently published protocol for His_6-tagged CK2α/CK2α′ was used instead (Werner et al. 2022).

4.5 Protein kinase assay

CK2 activity was determined by a capillary electrophoresis assay as previously reported (Gratz et al. 2010) with modifications. Briefly, 98 µl kinase buffer (150 mM NaCl, 25 mM $MgCl_2$, 25 mM Tris/HCl, pH 7.5) containing either 0.25 µg $CK2\alpha_2\beta_2$ or 0.5 µg of the catalytic subunits CK2α/CK2α′ was supplemented with 2 µl of the test compound dissolved in DMSO. After incubation for 10 min at 37 °C ($CK2\alpha_2\beta_2$) or 30 °C (CK2α/CK2α′) the kinase reaction was initiated by adding 100 µl assay buffer (150 mM NaCl, 25 mM $MgCl_2$, 228 µM substrate peptide RRRDDDSDDD, 120 µM ATP, 25 mM Tris/HCl, pH 7.5). After 15 min at 37 °C ($CK2\alpha_2\beta_2$) or 12 min at 30 °C (CK2α/CK2α′), the reaction was stopped by adding 25 µl EDTA (0.5 M, pH 8.0).

For the determination of IC_{50} values, dose-dependent activity determinations were performed with test compound concentrations ranging from 1 nM to 10 µM. A control without test compound, but the same volume of DMSO corresponded to 100 % activity. IC_{50} values were calculated by GraphPad Prism 5 (La Jolla, CA, USA).

In order to determine the mode of inhibition and K_i values of the compounds for CK2α, Michaelis-Menten kinetics was recorded at different test compound concentrations. To maintain steady-state conditions at all ATP concentrations, enzyme activities were determined over a period of 12 min at 30 °C. In addition, the final concentration of the substrate peptide RRRDDDSDDD was increased to 300 µM in these experiments. The resulting data points were plotted according to Hanes-Woolf using GraphPad Prism 5 (Hanes 1932).

4.6 Crystallization and crystal structure determination

4.6.1 Protein preparation and crystallization

For crystallization experiments with CK2α, we expressed and purified the C terminally-truncated, but fully active, $CK2\alpha^{1-335}$ (Ermakova et al. 2003). For the crystallization of **MC11** with CK2α′ we used the point mutant $CK2\alpha'^{Cys336Ser}$. Introducing this point mutation into CK2α′ prevents aggregation during purification (Bischoff et al. 2011). Transformation, expression and purification of both isoenzymes were carried out according to a previously reported protocol (Werner et al. 2022). Proteins were concentrated to 5–6 mg/ml in a 500 mM NaCl, 25 mM TRIS-HCl, pH 8.5 buffer for crystallization setups.

In this work, three crystal structures were reported. The CK2α′ co-crystal structure was prepared by applying a previously published back-soaking protocol (Lindenblatt et al. 2019; Werner et al. 2023) using the sitting-drop variant of vapor diffusion crystallization. For this, we initially prepared co-crystals of CK2α′ and the ATP-competitive inhibitor **MB002** (Maria Bretner, Warsaw). Firstly, **MB002** (10 mM stock solution in DMSO) was added to CK2α′ yielding a solution of 1 mM **MB002** in 5 mg/ml CK2α′. This was incubated on ice for 30 min followed by a short centrifugation step to remove any precipitate. The reservoir solution was composed of 900 mM LiCl, 100 mM TRIS-HCl, pH 8.5 and 28 % (*w*/*v*). We used 700 µl of this solution for every reservoir. The initial drop was composed of 4 µl of the protein/**MB002** mixture and 2 µl reservoir solution. After equilibration crystals were optimized by micro- and macro-seeding. Grown crystals were then used for back-soaking in reservoir solution mixed in a 4:1 ratio with a 10 mM solution of **MC11** in DMSO yielding a final concentration of 2 mM **MC11**.

CK2α was crystallized with **MC11** by co-crystallization in a low-salt and in a high-salt condition using the sitting-drop variant of vapor diffusion crystallization. The high-salt reservoir solution was composed of 4.2 M NaCl and 0.1 M citric acid adjusted to pH 5.5 with NaOH. $CK2\alpha^{1-335}$ was mixed with a 10 mM stock of **MC11** in DMSO to final concentrations of 1 mM **MC11** and 5 mg/ml $CK2\alpha^{1-335}$. After 30 min of incubation on ice we removed any precipitate by centrifugation. 1 µl of the supernatant was mixed with 1 µl of the high-salt reservoir solution and equilibrated against 700 µl of the reservoir solution. Crystal growth occurred spontaneously.

4.6.2 Data collection and processing

Co-crystals of **MC11** and CK2α' were cryo-protected by briefly incubating the crystals in a mix of 1.4 µl of their respective reservoir solution and 0.7 µl ethylene glycol prior to freezing the crystals in liquid nitrogen. Crystals grown in the high-salt crystallization condition were flash-frozen directly. Data collections were carried out at beamlines ID23-2 and ID30B of the ESRF (Grenoble, France). Diffraction data derived from the CK2α'/**MC11** crystal were processed using the autoPROC pipeline (Vonrhein et al. 2011), which applies XDS (Kabsch 2010), Pointless and Aimless (Evans and Murshudov 2013) from the ccp4 suite (Winn et al. 2011) and lastly Staraniso (Tickle et al. 2018). Data related to the high-salt co-crystal of

CK2α and **MC11** were manually processed in XDS (Kabsch 2010) and in Pointless and Aimless (Evans and Murshudov 2013) from the ccp4 suite (Winn et al. 2011). All phases were solved by molecular replacement using PHASER (McCoy et al. 2007) from Phenix (Adams et al. 2010). For the CK2α structure 2PVR (Niefind et al. 2007) from the PDB (Berman et al. 2000) was used as the search model, while PDB structure 6HMQ was used as the search model for the CK2α' structure. Refinement was conducted either manually in Coot (Emsley et al. 2010) or automated in the phenix.refine (Afonine et al. 2012) module of Phenix. Parameters and restraints of **MC11** were prepared in elbow (Moriarty et al. 2009).

The crystal structures are deposited in the PDB with the following codes: 9H97 ($CK2\alpha^{1\text{-}335}$/**MC11** crystallized under high-salt conditions), 9H9D ($CK2\alpha^{1\text{-}335}$/**MC11** crystallized under low-salt conditions) and 9H96 ($CK2\alpha'^{Cys336Ser}$/**MC11**) (Table S1).

4.7 Cytotoxicity test on leukemia cell lines and non-cancerous cell lines

4.7.1 Maintenance of cell lines

The acute myeloid leukemia (AML) cell lines MOLM-13 (DSMZ, ACC-554, and Matsuo et al. 1997) and MOLM-13 shp53 (Myhren et al. 2013) were cultured in RPMI medium enriched containing 10 % fetal bovine serum (FBS, Invitrogen, Carlsbad, CA, USA), whereas the MV4-11 cells (Quentmeier et al. 2003) were cultured in Iscove's medium supplemented with 8 mM L-glutamine and 10 % FBS. The rat acute promyelocytic leukemia (APL) cell lines IPC-81 (Lacaze et al. 1983) and IPC with enforced expression of Bcl-2 (Séité et al. 2000) were cultured in Dulbecco's Modified Eagles Medium (DMEM) supplemented with 10 % horse serum (Invitrogen, Carlsbad, CA, USA), and the human APL cell line NB4 (Lanotte et al. 1991) was cultured in RPMI medium containing 10 % FBS. The chronic myeloid leukemia (CML) cell line K562 (ATCC: CCL-243) was cultured similarly to the MV4-11 cells. The NRK normal rat kidney epithelial cells (ATCC: CRL-6509) were cultured in DMEM medium supplemented with 10 % FBS. All cell media were supplemented with 100 IU/ml penicillin and 0.1 mg/ml streptomycin (Cambrex, Verviers, Belgium) and cultured in a humidified atmosphere (37 °C, 5 % CO_2). All cell media were from Sigma (Sigma, La Jolla, CA, USA). The cell suspensions were cultured in tissue culture flasks at a density ranging between 70 and 800×10^3 cells/ml. The adherent NRK cells were cultured in monolayer, and when reaching more than 90 % confluence, detached by mild trypsin treatment for 4 min, centrifuged at $120 \times G$ and reseeded at 15–20 % confluence. Tests for mycoplasma infection were done for all cell lines twice during the period of the experiments, using the manufacturer's protocol (MycoAlert™, www.invivogen.com/mycostrip). No mycoplasma infection was detected for the duration of the experiments.

4.7.2 Cytotoxicity tests

The cell lines were seeded in 96-well tissue culture plates at 150,000 cells/ml and 0.1 ml/well. The adherent NRK cells were seeded the day before the experiment and left overnight in the incubator to attach to the substratum. The cells were exposed to 30 or 100 μM of CK2 inhibitors for 24 h before assessment of viability by the reporter dye WST-1 as described by the supplier (Roche Diagnostics, Basel, Switzerland). The cells were next fixed in 2 % buffered formaldehyde (pH 7.4) with the DNA-specific dye Hoechst 33342 (Polysciences Inc., Eppelheim, Germany) and scored for apoptosis and necrosis as previously described (Bjørnstad et al. 2019). Since CK2-inhibition can affect the activity of the enzyme which converts WST-1 into the reporter dye (Park et al. 2001), we found some instances where addition of CK2 inhibitors increased the WST-1 signal despite the presence of apoptotic nuclei. Therefore, only microscopic evaluation of nuclear morphology was used to assess cytotoxicity.

Acknowledgments: The authors thank eng. Nina Lied Larsen for help with cell culturing and cytotoxicity experiments. Christelle Marminon thanks Marine Cavaz for her help with chemistry. Marc Le Borgne and Christelle Marminon would like to thank "Institut Convergence PLAsCAN" (ANR-17-CONV-0002). We would also like to thank Brigitte Manship for editing the manuscript. The authors are grateful to Professor Ulrich Baumann, Cologne, for access to the Cologne Crystallisation facility (http://C2f.uni-koeln.de) which was installed by support from the Deutsche Forschungsgemeinschaft (DFG) (grant no. INST 216/682-1 FUGG). Further, we thank the staff of the European Synchrotron Radiation Facility (ESRF) in Grenoble (beamlines ID30b and ID23-2) and of the European Molecular Biology Laboratory (EMBL) at DESY in Hamburg (beamline P13) for assistance with X-ray diffraction data collection.
Research ethics: Not applicable.
Informed consent: Not applicable.
Author contributions: Experiments (A.G., A.M., C.M., C.W., D.A., D.L., J.C., L.H.); data analysis (A.G., A.M., C.M., C.W., D.A., D.L., J.J., K.N., L.H.); manuscript writing (A.G., C.M., D.A., C.W, K.N., L.H., M.L.B.); review and editing (C.M., J.J., K.N., L.H., M.L.B.); project administration (J.J., K.N., M.L.B., S.O.D.); funding acquisition (J.J., K.N., M.L.B., S.O.D.).

Use of Large Language Models, AI and Machine Learning Tools: None declared.

Conflict of interest: The authors state no conflict of interest.

Research funding: This research was funded by the Agence Nationale de la Recherche (ANR), grant no. ANR-22-CE92-0081-01. This research was funded by the Deutsche Forschungsgemeinschaft (DFG), grants nos. NI 643/4-2 and NI 643/11-1 to K.N. and grant no. JO 183/10-1 to J.J.

Data availability: Not applicable.

References

Adams, P.D., Afonine, P.V., Bunkóczi, G., Chen, V.B., Davis, I.W., Echols, N., Headd, J.J., Hung, L.W., Kapral, G.J., Grosse-Kunstleve, R.W., et al. (2010). PHENIX: a comprehensive python-based system for macromolecular structure solution. *Acta Crystallogr. D Biol. Crystallogr.* 66: 213–221.

Afonine, P.V., Grosse-Kunstleve, R.W., Echols, N., Headd, J.J., Moriarty, N.W., Mustyakimov, M., Terwilliger, T.C., Urzhumtsev, A., Zwart, P.H., and Adams, P.D. (2012). Towards automated crystallographic structure refinement with phenix.refine. *Acta Crystallogr. D Biol. Crystallogr.* 68: 352–367.

Allen, J.R., Burli, R., Golden, J.E., Muller, K.M., and Reed, A.B. (2008). Preparation of indanone derivatives as prolyl hydroxylase inhibitors. WO2008130508, Available at: https://patentscope.wipo.int/search/en/detail.jsf?docId=WO2008130508.

Berman, H.M., Westbrook, J., Feng, Z., Gilliland, G., Bhat, T.N., Weissig, H., Shindyalov, I.N., and Bourne, P.E. (2000). The protein data bank. *Nucleic Acids Res.* 28: 235–242.

Birus, R., El-Awaad, E., Ballentin, L., Alchab, F., Aichele, D., Ettouati, L., Götz, C., Le Borgne, M., and Jose, J. (2022). 4,5,7-Trisubstituted indeno[1,2-*b*]indole inhibits CK2 activity in tumor cells equivalent to CX-4945 and shows strong anti-migratory effects. *FEBS Open Bio* 12: 394–411.

Bischoff, N., Olsen, B., Raaf, J., Bretner, M., Issinger, O.G., and Niefind, K. (2011). Structure of the human protein kinase CK2 catalytic subunit CK2α′ and interaction thermodynamics with the regulatory subunit CK2β. *J. Mol. Biol.* 407: 1–12.

Bjørnstad, R., Aesoy, R., Bruserud, Ø., Brenner, A.K., Giraud, F., Dowling, T.H., Gausdal, G., Moreau, P., Døskeland, S.O., Anizon, F., et al. (2019). A kinase inhibitor with anti-pim kinase activity is a potent and selective cytotoxic agent toward acute myeloid leukemia. *Mol. Cancer Ther.* 18: 567–578.

Borgo, C., D'Amore, C., Sarno, S., Salvi, M., and Ruzzene, M. (2021). Protein kinase CK2: a potential therapeutic target for diverse human diseases. *Signal Transduct. Targeted Ther.* 6: 183.

Bouzina, A., Berredjem, M., Nocentini, A., Bua, S., Bouaziz, Z., Jose, J., Le Borgne, M., Marminon, C., Gratteri, P., and Supuran, C. (2021). Ninhydrins inhibit carbonic anhydrases directly binding to the metal ion. *Eur. J. Med. Chem.* 209: 112875–112882.

Bretner, M., Najda-Bernatowicz, A., Łebska, M., Muszyńska, G., Kilanowicz, A., and Sapota, A. (2008). New inhibitors of protein kinase CK2, analogues of benzimidazole and benzotriazole. *Mol. Cell. Biochem.* 316: 87–89.

Castello, J., Ragnauth, A., Friedman, E., and Rebholz, H. (2017). CK2-an emerging target for neurological and psychiatric disorders. *Pharmaceuticals* 10: 7.

Chen, Y., Wang, Y., Wang, J., Zhou, Z., Cao, S., and Zhang, J. (2023). Strategies of targeting CK2 in drug discovery: challenges, opportunities, and emerging prospects. *J. Med. Chem.* 66: 2257–2281.

Chojnacki, K., Lindenblatt, D., Wińska, P., Wielechowska, M., Toelzer, C., Niefind, K., and Bretner, M. (2021). Synthesis, biological properties and structural study of new halogenated azolo[4,5-*b*]pyridines as inhibitors of CK2 kinase. *Bioorg. Chem.* 106: 104502.

Cozza, G. (2017). The development of CK2 inhibitors: from traditional pharmacology to in silico rational drug design. *Pharmaceuticals* 10: 26.

Daina, A., Michielin, O., and Zoete, V. (2017). SwissADME: a free web tool to evaluate pharmacokinetics, drug-likeness and medicinal chemistry friendliness of small molecules. *Sci. Rep.* 7: 42717.

Delaney, J.S. (2004). ESOL: estimating aqueous solubility directly from molecular structure. *J. Chem. Inf. Comput. Sci.* 44: 1000–1005.

Emsley, P., Lohkamp, B., Scott, W.G., and Cowtan, K. (2010). Features and development of coot. *Acta Crystallogr. D Biol. Crystallogr.* 66: 486–501.

Ermakova, I., Boldyreff, B., Issinger, O.G., and Niefind, K. (2003). Crystal structure of a C-terminal deletion mutant of human protein kinase CK2 catalytic subunit. *J. Mol. Biol.* 330: 925–934.

Evans, P.R. and Murshudov, G.N. (2013). How good are my data and what is the resolution? *Acta Crystallogr. D Biol. Crystallogr.* 69: 1204–1214.

Golub, A.G., Yakovenko, O.Y., Bdzhola, V.G., Sapelkin, V.M., Zien, P., and Yarmoluk, S.M. (2006). Evaluation of 3-carboxy-4(1H)-quinolones as inhibitors of human protein kinase CK2. *J. Med. Chem.* 49: 6443–6450.

Golub, A.G., Bdzhola, V.G., Kyshenia, Y.V., Sapelkin, V.M., Prykhod'ko, A.O., Kukharenko, O.P., Ostrynska, O.V., and Yarmoluk, S.M. (2011). Structure-based discovery of novel flavonol inhibitors of human protein kinase CK2. *Mol. Cell. Biochem.* 356: 107–115.

Götz, C., Gratz, A., Kucklaender, U., and Jose, J. (2012). TF-a novel cell-permeable and selective inhibitor of human protein kinase CK2 induces apoptosis in the prostate cancer cell line LNCaP. *Biochim. Biophys. Acta* 1820: 970–977.

Gratz, A., Gotz, C., and Jose, J. (2010). A CE-based assay for human protein kinase CK2 activity measurement and inhibitor screening. *Electrophoresis* 31: 634–640.

Haidar, S., Marminon, C., Aichele, D., Nacereddine, A., Zeinyeh, W., Bouzina, A., Berredjem, M., Ettouati, L., Bouaziz, Z., Le Borgne, M., et al. (2020). QSAR model of indeno[1,2-*b*]indole derivatives and identification of *N*-isopentyl-2-methyl-4,9-dioxo-4,9-dihydronaphtho[2,3-*b*]furan-3-carboxamide. *Molecules* 25: 97.

Hanes, C.S. (1932). Studies on plant amylases: the effect of starch concentration upon the velocity of hydrolysis by the amylase of germinated barley. *Biochem. J.* 26: 1406–1421.

Hemmerling, H.J. and Reiss, G. (2009). Partially saturated indeno[1,2-*b*] indole derivatives via deoxygenation of heterocyclic α-hydroxy-N,O-hemiaminals. *Synthesis* 6: 985–999.

Hochscherf, J., Lindenblatt, D., Witulski, B., Birus, R., Aichele, D., Marminon, C., Bouaziz, Z., Le Borgne, M., Jose, J., and Niefind, K. (2017). Unexpected binding mode of a potent indeno[1,2-*b*]indole-type inhibitor of protein kinase CK2 revealed by complex structures with the catalytic subunit CK2α and its paralog CK2α. *Pharmaceuticals* 10: 98.

Hundsdörfer, C., Hemmerling, H.J., Götz, C., Totzke, F., Bednarski, P., Le Borgne, M., and Jose, J. (2012). Indeno[1,2-*b*]indole derivatives as a novel class of potent human protein kinase CK2 inhibitors. *Bioorg. Med. Chem.* 20: 2282–2289.

Jabor Gozzi, G., Bouaziz, Z., Winter, E., Daflon-Yunes, N., Aichele, A., Nacereddine, A., Marminon, C., Valdameri, G., Zeinyeh, W., Bollacke, A., et al. (2015). Converting potent indeno[1,2-*b*]indole inhibitors of protein kinase CK2 into selective inhibitors of the breast cancer resistance protein ABCG2. *J. Med. Chem.* 58: 265–277.

Kabsch, W. (2010). XDS. *Acta Crystallogr. D Biol. Crystallogr.* 66: 125–132.

Lacaze, N., Gombaud-Saintonge, G., and Lanotte, M. (1983). Conditions controlling long-term proliferation of Brown Norway rat promyelocytic leukemia in vitro: primary growth stimulation by microenvironment and establishment of an autonomous Brown Norway 'leukemic stem cell line'. *Leuk. Res.* 7: 145–154.

Lanotte, M., Martin-Thouvenin, V., Najman, S., Balerini, P., Valensi, F., and Berger, R. (1991). NB4, a maturation inducible cell line with t(15;17) marker isolated from a human acute promyelocytic leukemia (M3). *Blood* 77: 1080–1086.

Lindenblatt, D., Nickelsen, A., Applegate, V.M., Hochscherf, J., Witulski, B., Bouaziz, Z., Marminon, C., Bretner, M., Le Borgne, M., Jose, J., et al. (2019). Diacritic binding of an indenoindole inhibitor by CK2α paralogs explored by a reliable path to atomic resolution CK2α′ structures. *ACS Omega* 4: 5471–5478.

Lindenblatt, D., Applegate, V., Nickelsen, A., Klußmann, M., Neundorf, I., Götz, C., Jose, J., and Niefind, K. (2022). Molecular plasticity of crystalline CK2α′ leads to KN2, a bivalent inhibitor of protein kinase CK2 with extraordinary selectivity. *J. Med. Chem.* 65: 1302–1312.

Lipinski, C.A., Lombardo, F., Dominy, B.W., and Feeney, P.J. (2001). Experimental and computational approaches to estimate solubility and permeability in drug discovery and development settings. *Adv. Drug Deliv. Rev.* 46: 3–26.

Litchfield, D.W. (2003). Protein kinase CK2: structure, regulation and role in cellular decisions of life and death. *Biochem. J.* 369: 1–15.

Makowska, M., Łukowska-Chojnacka, E., Wińska, P., Kuś, A., Bilińska-Chomik, A., and Bretner, M. (2011). Design and synthesis of CK2 inhibitors. *Mol. Cell. Biochem.* 356: 91–96.

Marminon, C., Nacereddine, A., Bouaziz, Z., Nebois, P., Jose, J., and Le Borgne, M. (2015). Microwave-assisted oxidation of indan-1-ones into ninhydrines. *Tetrahedron Lett*. 56: 1840–1842.

Matsuo, Y., MacLeod, R.A.F., Uphoff, C.C., Drexler, H.G., Nishizaki, C., Katayama, Y., Kimura, G., Fujii, N., Omoto, E., Harada, M., et al. (1997). Two acute monocytic leukemia (AML-M5a) cell lines (MOLM-13 and MOLM-14) with interclonal phenotypic heterogeneity showing *MLL-AF9* fusion resulting from an occult chromosome insertion, ins(11; 9)(q23;p22p23). *Leukemia* 11: 1469–1477.

Mazzorana, M., Pinna, L.A., and Battistutta, R. (2008). A structural insight into CK2 inhibition. *Mol. Cell. Biochem.* 316: 57–62.

McCoy, A.J., Grosse-Kunstleve, R.W., Adams, P.D., Winn, M.D., Storoni, L.C., and Read, R.J. (2007). Phaser crystallographic software. *J. Appl. Crystallogr.* 40: 658–674.

Meggio, F. and Pinna, L.A. (2003). One-thousand-and-one substrates of protein kinase CK2? *FASEB J.* 17: 349–368.

Moriarty, N.W., Grosse-Kunstleve, R.W., and Adams, P.D. (2009). Electronic ligand builder and optimization workbench (eLBOW): a tool for ligand coordinate and restraint generation. *Acta Crystallogr. D Biol. Crystallogr.* 65: 1074–1080.

Mosmann, T. (1983). Rapid colorimetric assay for cellular growth and survival: application to proliferation and cytotoxicity assays. *J. Immunol. Methods* 65: 55–63.

Myhren, L.E., Nygaard, G., Gausdal, G., Sletta, H., Teigen, K., Degnes, K.F., Zahlsen, K., Brunsvik, A., Bruserud, Ø., Døskeland, S.O., et al. (2013). Iodinin (1,6-dihydroxyphenazine 5,10-dioxide) from Streptosporangium sp. induces apoptosis selectively in myeloid leukemia cell lines and patient cells. *Mar. Drugs* 11: 332–349.

Niefind, K., Yde, C.W., Ermakova, I., and Issinger, O.G. (2007). Evolved to be active: sulfate ions define substrate recognition sites of CK2α and emphasise its exceptional role within the CMGC family of eukaryotic protein kinases. *J. Mol. Biol.* 370: 427–438.

Pagano, M.A., Andrzejewska, M., Ruzzene, M., Sarno, S., Cesaro, L., Bain, J., Elliott, M., Meggio, F., Kazimierczuk, Z., and Pinna, L.A. (2004a). Optimization of protein kinase CK2 inhibitors derived from 4,5,6,7-tetrabromobenzimidazole. *J. Med. Chem.* 47: 6239–6247.

Pagano, M.A., Meggio, F., Ruzzene, M., Andrzejewska, M., Kazimierczuk, Z., and Pinna, L.A. (2004b). 2-Dimethylamino-4,5,6,7-tetrabromo-1H-benzimidazole: a novel powerful and selective inhibitor of protein kinase CK2. *Biochem. Biophys. Res. Commun.* 321: 1040–1044.

Pagano, M.A., Poletto, G., Di Maira, G., Cozza, G., Ruzzene, M., Sarno, S., Bain, J., Elliott, M., Moro, S., Zagotto, G., et al. (2007). Tetrabromocinnamic acid (TBCA) and related compounds represent a new class of specific protein kinase CK2 inhibitors. *ChemBioChem* 8: 129–139.

Pagano, M.A., Bain, J., Kazimierczuk, Z., Sarno, S., Ruzzene, M., Di Maira, G., Elliott, M., Orzeszko, A., Cozza, G., Meggio, F., et al. (2008). The selectivity of inhibitors of protein kinase CK2: an update. *Biochem. J.* 415: 353–365.

Park, H.S., Lee, S.M., Lee, J.H., Kim, Y.S., Bae, Y.S., and Park, J.W. (2001). Phosphorylation of the leucocyte NADPH oxidase subunit p47(phox) by casein kinase 2: conformation-dependent phosphorylation and modulation of oxidase activity. *Biochem. J.* 358: 783–790.

Quentmeier, H., Reinhardt, J., Zaborski, M., and Drexler, H.G. (2003). FLT3 mutations in acute myeloid leukemia cell lines. *Leukemia* 17: 120–124.

Quezada Meza, C.P. and Ruzzene, M. (2023). Protein kinase CK2 and SARS-CoV-2: an expected interplay story. *Kinases Phosphatases* 1: 141–150.

Rongved, P., Kirsch, G., Bouaziz, Z., Jose, J., and Le Borgne, M. (2013). Indenoindoles and cyclopentacarbazoles as bioactive compounds: synthesis and biological applications. *Eur. J. Med. Chem.* 69: 465–479.

Ruzzene, M. and Pinna, L.A. (2010). Addiction to protein kinase CK2: a common denominator of diverse cancer cells? *Biochim. Biophys. Acta* 1804: 499–504.

Sarno, S., Reddy, H., Meggio, F., Ruzzene, M., Davies, S.P., Donella-Deana, A., Shugar, D., and Pinna, L.A. (2001). Selectivity of 4,5,6,7-tetrabromobenzotriazole, an ATP site-directed inhibitor of protein kinase CK2 ('casein kinase-2'). *FEBS Lett.* 496: 44–48.

Schnitzler, A., Gratz, A., Bollacke, A., Weyrich, M., Kuckländer, U., Wünsch, B., Götz, C., Niefind, K., and Jose, J. (2018). A π-halogen bond of dibenzofuranones with the gatekeeper Phe113 in human protein kinase CK2 leads to potent tight binding inhibitors. *Pharmaceuticals* 11: 23.

Séité, P., Ruchaud, S., Hillion, J., Gendron, M.C., Bruland, O., Ségal-Bendirdjian, E., Doskeland, S.O., Lillehaug, J.R., and Lanotte, M. (2000). Ectopic expression of Bcl-2 switches over nuclear signalling for cAMP-induced apoptosis to granulocytic differentiation. *Cell Death Differ*. 7: 1081–1089.

Tickle, I.J., Flensburg, C., Keller, P., Paciorek, W., Sharff, A., Vonrhein, C., and Bricogne, G. (2018). *Staraniso*. Global Phasing Ltd., Cambridge, UK.

Trembley, J.H., Kren, B.T., Afzal, M., Scaria, G.A., Klein, M.A., and Ahmed, K. (2023). Protein kinase CK2 – diverse roles in cancer cell biology and therapeutic promise. *Mol. Cell. Biochem.* 478: 899–926.

Vonrhein, C., Flensburg, C., Keller, P., Sharff, A., Smart, O., Paciorek, W., Womack, T., and Bricogne, G. (2011). Data processing and analysis with the autoPROC toolbox. *Acta Crystallogr. D Biol. Crystallogr.* 67: 293–302.

Werner, C., Gast, A., Lindenblatt, D., Nickelsen, A., Niefind, K., Jose, J., and Hochscherf, J. (2022). Structural and enzymological evidence for an altered substrate specificity in Okur-Chung neurodevelopmental syndrome mutant CK2α^{Lys198Arg}. *Front. Mol. Biosci.* 9: 831693.

Werner, C., Lindenblatt, D., Viht, K., Uri, A., and Niefind, K. (2023). Discovery and exploration of protein kinase CK2 binding sites using

CK2α′^{Cys336Ser} as an exquisite crystallographic tool. *Kinases Phosphatases* 1: 306–322.

Winiewska-Szajewska, M., Maciejewska, A.M., Speina, E., Poznanski, J., and Paprocki, D. (2021). Synthesis of novel halogenated heterocycles based on *o*-phenylenediamine and their interactions with the catalytic subunit of protein kinase CK2. *Molecules* 26: 3163.

Winn, M.D., Ballard, C.C., Cowtan, K.D., Dodson, E.J., Emsley, P., Evans, P.R., Keegan, R.M., Krissinel, E.B., Leslie, A.G., McCoy, A., et al. (2011). Overview of the CCP4 suite and current developments. *Acta Crystallogr. D Biol. Crystallogr.* 67: 235–242.

Zandomeni, R., Zandomeni, M.C., Shugar, D., and Weinmann, R. (1986). Casein kinase type II is involved in the inhibition by 5,6-dichloro-1-β-D-ribofuranosylbenzimidazole of specific RNA polymerase II transcription. *J. Biol. Chem.* 261: 3414–3419.

Zień, P., Duncan, J.S., Skierski, J., Bretner, M., Litchfield, D.W., and Shugar, D. (2005). Tetrabromobenzotriazole (TBBt) and tetrabromobenzimidazole (TBBz) as selective inhibitors of protein kinase CK2: evaluation of their effects on cells and different molecular forms of human CK2. *Biochim. Biophys. Acta Proteins Proteom.* 1754: 271–280.

Supplementary Material: This article contains supplementary material (https://doi.org/10.1515/hsz-2024-0160).